Anthraquinone Derivatives in Aqueous Flow Batteries

*Michael R. Gerhardt, Liuchuan Tong, Rafael Gómez-Bombarelli, Qing Chen, Michael P. Marshak, Cooper J. Galvin, Alán Aspuru-Guzik, Roy G. Gordon, and Michael J. Aziz**

Anthraquinone derivatives are being considered for large scale energy storage applications because of their chemical tunability and rapid redox kinetics. The authors investigate four anthraquinone derivatives as negative electrolyte candidates for an aqueous quinone-bromide redox flow battery: anthraquinone-2-sulfonic acid (AQS), 1,8-dihydroxyanthraquinone-2,7-disulfonic acid (DHAQDS), alizarin red S (ARS), and 1,4-dihydroxyanthraquinone-2,3-dimethylsulfonic acid (DHAQDMS). The standard reduction potentials are all lower than that of anthraquinone-2,7-disulfonic acid (AQDS), the molecule used in previous quinone-bromide batteries. DHAQDS and ARS undergo irreversible reactions on contact with bromine, which precludes their use against bromine but not necessarily against other electrolytes. DHAQDMS is apparently unreactive with bromine but cannot be reversibly reduced, whereas AQS is stable against bromine and stable upon reduction. The authors demonstrate an AQS-bromide flow cell with higher open circuit potential and peak galvanic power density than the equivalent AQDS-bromide cell. This study demonstrates the use of chemical synthesis to tailor organic molecules for improving flow battery performance.

1. Introduction

Electric grids are vulnerable to mismatched electricity supply and demand. Grid inflexibility leads to capital expenditures for power plants that operate only rarely, near peak demand, and is anticipated to hinder massive penetration of intermittent renewable sources, such as wind and solar power. Redox flow batteries (RFBs) provide a safe and potentially cost-effective method of bulk electricity storage, which could solve the intermittency problem.[1] RFBs hold advantages over conventional batteries, including the independent scaling of energy and power, which enables long discharge durations at rated power; and the use of liquid redox-active species, which enables long cycle life by avoiding mechanical strain during cycling.[2] The most widely deployed RFB technology is the all-vanadium RFB, with over 20 demonstration systems —some as large as 4 MW/6 MWh.[3] The high and variable price of vanadium, however, renders these batteries too expensive and risky for wide scale commercialization.[4]

Inexpensive derivatives of quinones have been explored as alternatives to vanadium as the electroactive species in aqueous flow batteries, as quinones have rapid redox kinetics and chemical tunability.[5–7] Combinatorial theoretical studies have identified thousands of quinone derivatives with varying electrochemical and chemical properties, representing an immense range of possible vanadium alternatives.[8]

The low open-circuit voltage (OCV) of quinone-bromide RFBs, relative to vanadium RFBs, limits their performance. Vanadium flow batteries have an OCV of 1.5 V with the highest reported peak galvanic power density reaching over 1.3 W cm^{-2}; in contrast, the highest reported performance from quinone-based batteries is an OCV of 0.94 V and a peak power density of 1.0 W cm^{-2} using elevated temperature (40 °C) and excess Br_2 content.[9,10]

The OCV and peak power density of the quinone-bromide flow battery can be increased by using a quinone with a lower reduction potential than that of anthraquinone-2,7-disulfonic acid (AQDS), which is the molecule previously employed in the quinone-bromide flow battery.[6,9,11,12] Chemical principles suggest that removing one of the electron-withdrawing sulfonate groups from AQDS should lower the reduction potential, thereby raising the OCV of the cell. Previous experimental and computational studies have also suggest attaching electron-donating hydroxy groups to lower the reduction potential of the molecule.[6,8,13]

In this paper, both the removal of sulfonate groups and the addition of hydroxy groups were investigated in order to increase

M. R. Gerhardt, Dr. Q. Chen, Prof. R. G. Gordon, Prof. M. J. Aziz
Harvard John A. Paulson School of Engineering and Applied Sciences
Cambridge, MA 02138, USA
E-mail: maziz@harvard.edu
L. Tong, Dr. R. Gómez-Bombarelli, Prof. A. Aspuru-Guzik, Prof. R. G. Gordon
Department of Chemistry and Chemical Biology
Harvard University
Cambridge, MA 02138, USA
Prof. M. P. Marshak
Department of Chemistry and Biochemistry
University of Colorado Boulder
Boulder, CO 80309, USA
C. J. Galvin
Biophysics Program
Stanford University
Stanford, CA 94305, USA

DOI: 10.1002/aenm.201601488

the voltage of quinone-bromide flow batteries. Two synthesized anthraquinone derivatives, 1,8-dihydroxyanthraquinone-2,7-disulfonic acid (DHAQDS) and 1,4-dihydroxyanthraquinone 2,3-dimethylsulfonic acid (DHAQDMS), were evaluated for use in a quinone-bromide flow battery alongside the commercially available anthraquinone-2-sulfonic acid (AQS). These anthraquinone derivatives have lower reduction potentials than AQDS. DHAQDS and DHAQDMS have not been previously demonstrated in a flow battery. Although AQS has been demonstrated in a flow battery with a tiron posolyte (positive electrolyte),[7] it has not been demonstrated in a flow battery with a bromine-bearing posolyte. Each quinone was tested for chemical stability against irreversible bromination. We evaluate the electrochemical cyclability of AQS and the newly synthesized DHAQDS and DHAQDMS in flow cells against AQDS and compare to that of AQDS against itself. Finally, we establish AQS as a potential negolyte (negative electrolyte) for use with the bromine/hydrobromic acid posolyte by demonstrating cycling of an AQS-bromide cell.

2. Tuning of Quinone Reduction Potential and Cell Voltage

In **Figure 1**a we show the tuning of the reduction potential through manipulating the functional groups attached to the molecule. For example, AQS exhibits a slightly lower reduction potential than AQDS, due to the removal of one of the electron-withdrawing sulfonic acid groups. In addition, DHAQDS has a lower reduction potential than both AQS and AQDS, due to the installation of electron-donating hydroxy groups. Distancing the electron-withdrawing groups from the redox-active center, as seen in DHAQDMS, drops the reduction potential of the quinone even further.

Lowering the reduction potential of the quinone in the negolyte is expected to increase the cell OCV. To demonstrate this behavior, quinone-bromide flow cells were assembled using a negolyte containing 1 M quinone and 3 M total protons with a posolyte containing 3 M HBr and 0.5 M Br_2. All quinone-bromide full cells show the expected trend at low states of charge, as shown in Figure 1b. However, at higher states of charge, the OCV of DHAQDS and DHAQDMS cells falls from this trend. During cell operation, these reagents undergo distinct decomposition reactions, which restrict their usage in flow batteries. The next sections detail evidence for the irreversible destruction of DHAQDS by Br_2 but demonstrate the ability to reversibly cycle DHAQDS electrochemically. Conversely, although DHAQDMS seems to be stable in the presence of bromine, it cannot be electrochemically reduced and re-oxidized many times under the reaction conditions investigated here.

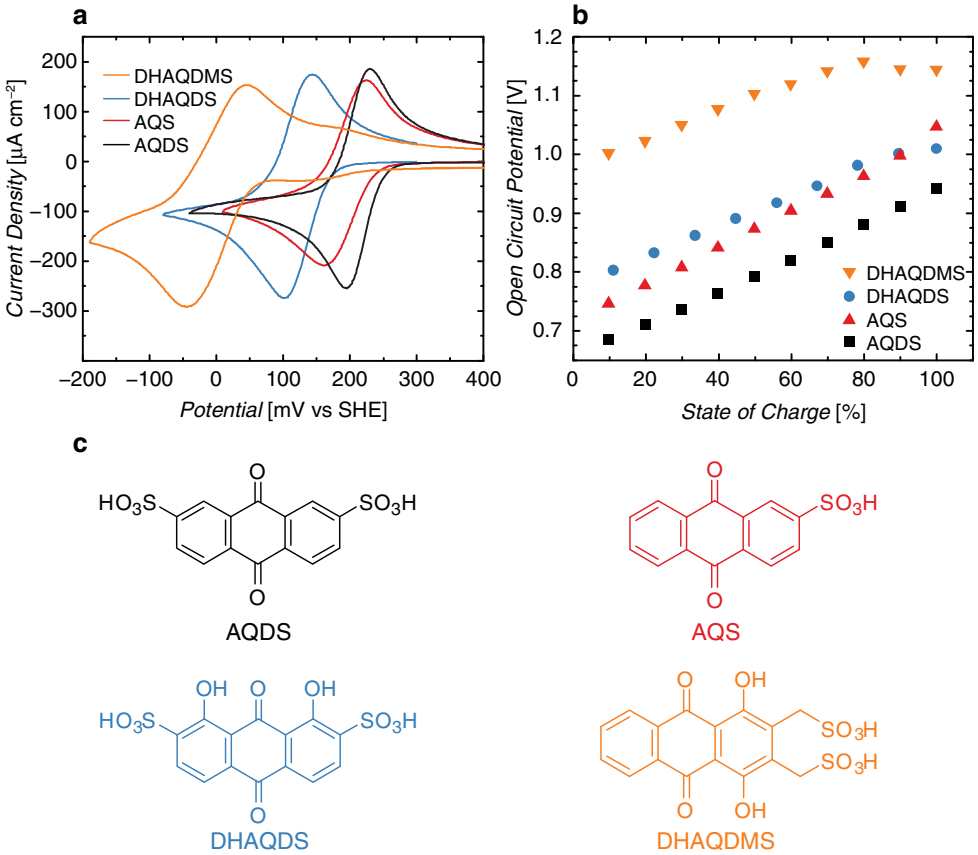

Figure 1. a) Cyclic voltammograms of AQDS (black), AQS (red), DHAQDS (blue), and DHAQDMS (orange), showing the decrease in reduction potential through chemical modification. b) Open circuit voltage as a function of state of charge for each quinone in a flow cell paired with the bromine-hydrobromic acid posolyte. c) Structures of AQDS, AQS, DHAQDS, and DHAQDMS.

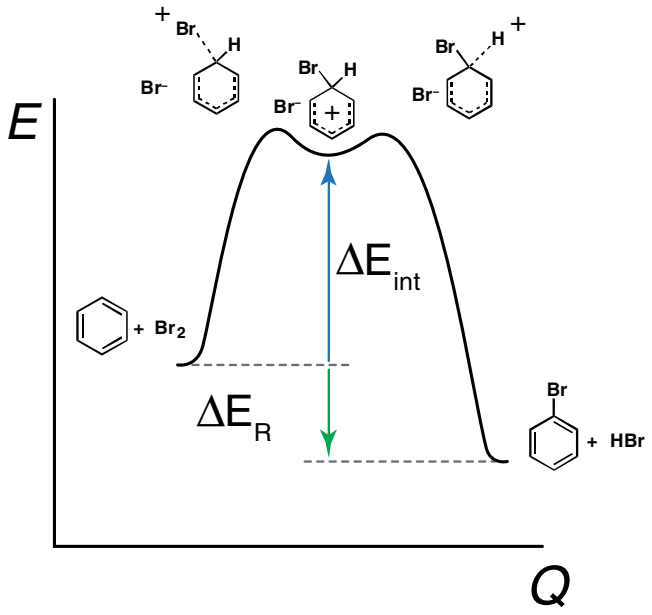

Figure 2. A schematic illustration of the energy landscape of electrophilic aromatic substitution on an aromatic ring, with relative energy (E) as a function of the reaction coordinate (Q). The energy change upon going from reactants to intermediate addition product, ΔE_{Int}, appears to correlate with stability against bromination of the quinones studied here.

3. Reactivity of Quinones with Bromine

Bromine can permeate the Nafion membrane, crossing from the posolyte to the negolyte at a small but non-negligible rate.[11,14] Therefore, molecules used in an RFB containing bromine species must survive a harsh chemical environment to minimize capacity fade from molecule destruction.

3.1. Calculation of Activation Energy for Electrophilic Aromatic Substitution

One possible reaction between anthraquinone derivatives and bromine is aromatic electrophilic substitution, in which bromine replaces a hydrogen atom attached to an aromatic carbon on the outer rings of the anthraquinone. If the activation barrier for bromination is large enough, anthraquinone derivatives may be kinetically stabilized and resist bromination despite a thermodynamic driving force in favor of bromination. Because a high-energy addition intermediate is formed in aromatic electrophilic addition, Hammond's principle suggests that the reaction barrier will be closely related to the formation energy of the non-aromatic cationic addition intermediate ΔE_{Int} (see **Figure 2**).[15] Furthermore, the barrier to bromination of the oxidized anthraquinone is the most relevant metric for determining irreversible reactivity with bromine, as bromine is likely to reversibly oxidize the reduced form of each anthraquinone derivative rather than substitute an exposed hydrogen on the aromatic ring.[16]

The activation energy for bromine substitution can be altered by attaching different functional groups to the anthraquinone molecule. For example, electron-withdrawing groups, such as sulfonate groups, raise the activation barrier and protect an aromatic ring from electrophilic substitution, whereas electron-donating hydroxy groups activate a ring.

The effect of the chemical substituent on the activation barrier for bromination can be computed quantitatively. The activation barriers for bromination were calculated relative to AQDS for four quinone derivatives, and these values are shown in **Table 1**. In addition to AQS, DHAQDS, and DHAQDMS, we chose to study alizarin red S (ARS), which has recently been demonstrated in a flow battery with a tiron posolyte.[17] The activation barrier for DHAQDS bromination is predicted to be 49 (PBE/6-31G*) to 77 (B3LYP/6-31G*) kJ mol^{-1} less than the barrier for AQDS bromination, which constitutes an acceleration in the rate of aromatic substitution of over 8–13 orders of magnitude, respectively, for DHAQDS at room temperature. ARS is predicted to be even less stable, and DHAQDMS is the only quinone derivative studied here that is predicted to be more stable than AQDS in its oxidized form.

3.2. Experimental Stability of Quinones against Bromination

The stability of AQDS against bromination was demonstrated previously via heating to 100 °C in mixtures of bromine and hydrobromic acid.[6] Bromine exposure tests were performed on AQS, DHAQDS, and alizarin red S (ARS). The latter has recently been demonstrated in an aqueous flow battery against

Table 1. Quantum-chemical predictions of stability of quinones and hydroquinones against bromination. ΔE_R is the energy change upon going from reactants to brominated product minus the corresponding change for AQDS; ΔE_{Int} is the energy change upon going from reactants to intermediate addition product minus the corresponding change for AQDS. Note: 5.7 kJ mol^{-1} corresponds to a factor of 10 in reaction rates at 298 K.

	PBE/6-31G*				B3LYP/6-31G*				
	ΔE_R [kJ mol^{-1}]		ΔE_{Int} [kJ mol^{-1}]		ΔE_R [kJ mol^{-1}]		ΔE_{Int} [kJ mol^{-1}]		
Molecule	Reduced form	Oxidized form	Reduced form	Oxidized form	Reduced form	Oxidized form	Reduced form	Oxidized form	Experimental stability
AQDS	0	0	0	0	0	0	0	0	Good
AQS	−20	−17	−51	−34	−25	−22	−72	−46	Good
DHAQDS	14	47	−50	−49	16	48	−65	−77	Poor
ARS	−22	−6	−91	−95	−28	−10	−105	−91	Poor
DHAQDMS	41	68	−74	9	38	74	−104	13	Apparently stable

a tiron posolyte and was chosen to test our hypothesis that irreversible reaction with bromine occurs.[17] ^{1}H NMR spectra were obtained before and after adding bromine to each sample to observe changes in the quinone molecules. The ^{1}H NMR spectra of AQS (**Figure 3**a,b) remained essentially unchanged after 24 h in excess bromine, indicating a reaction rate with bromine that is below the detection limit.

The DHAQDS proton NMR spectrum (Figure 3c) shows two peaks in a range typical of aromatic protons. These peaks correspond to the two unique positions of protons on the aromatic rings. Upon addition of bromine, however, these peaks disappear (Figure 3d), indicating reaction with DHAQDS. Furthermore, an orange solid precipitated. Elemental analysis of this precipitate suggests a polybrominated product with very little sulfur content, possibly indicating the loss of sulfonic acid groups and the addition of bromine to the aromatic rings (see the Supporting Information). Thus, DHAQDS appears to react irreversibly with bromine. Similarly, the aromatic proton peaks in the alizarin red S (ARS) spectrum disappear upon addition of bromine (Figure 3e–f). However, unlike DHAQDS, no precipitate was observed, indicating that the reaction product may remain soluble in water. These results agree with our prediction of stability against electrophilic aromatic substitution. The instability of DHAQDS and ARS to bromination can be explained by the presence of hydroxy groups increasing the electron density in the aromatic π system, making the rings more prone to electrophilic substitution.

The instability of DHAQDS and ARS in the presence of bromine highlights a challenge in producing low potential quinones for bromine flow batteries. As described above, the same functional groups that lower the reduction potential also increase the reactivity of these molecules with bromine. To address this problem we synthesized DHAQDMS, which has one unsubstituted aromatic ring and one fully substituted ring. These measures are predicted to prevent bromination, as discussed in the following section. DHAQDMS was synthesized in excess bromine, and exposure to bromine does not cause a precipitate. Bromine-free cycling experiments (**Figure 4**) reveal a limitation on the stability of the reduced form of DHAQDMS, which will be discussed in the next section. Because this instability of reduced DHAQDMS precludes its use in flow batteries, further bromine stability experiments were not performed.

4. Quinone Stability to Electrochemical Cycling

The electrochemical reversibility of the newly synthesized DHAQDS and DHAQDMS molecules was tested by cycling each molecule in a flow cell against a posolyte containing a mixture of reduced and oxidized AQDS. AQS and AQDS, which have already been demonstrated in cycling experiments,[7,12] were also tested to validate the measurement method. The cell operated with a large excess of posolyte (1 M total AQDS and H_2AQDS, 30 mL) relative to negolyte (0.01 M test quinone, 20 mL) to ensure that the entirety of the negolyte can be charged and discharged.

Constant-current cycling (Figure 4a, voltage traces available in Figure S2 in the Supporting Information) shows that AQDS and AQS are cyclable at relatively high rates. Cycling at

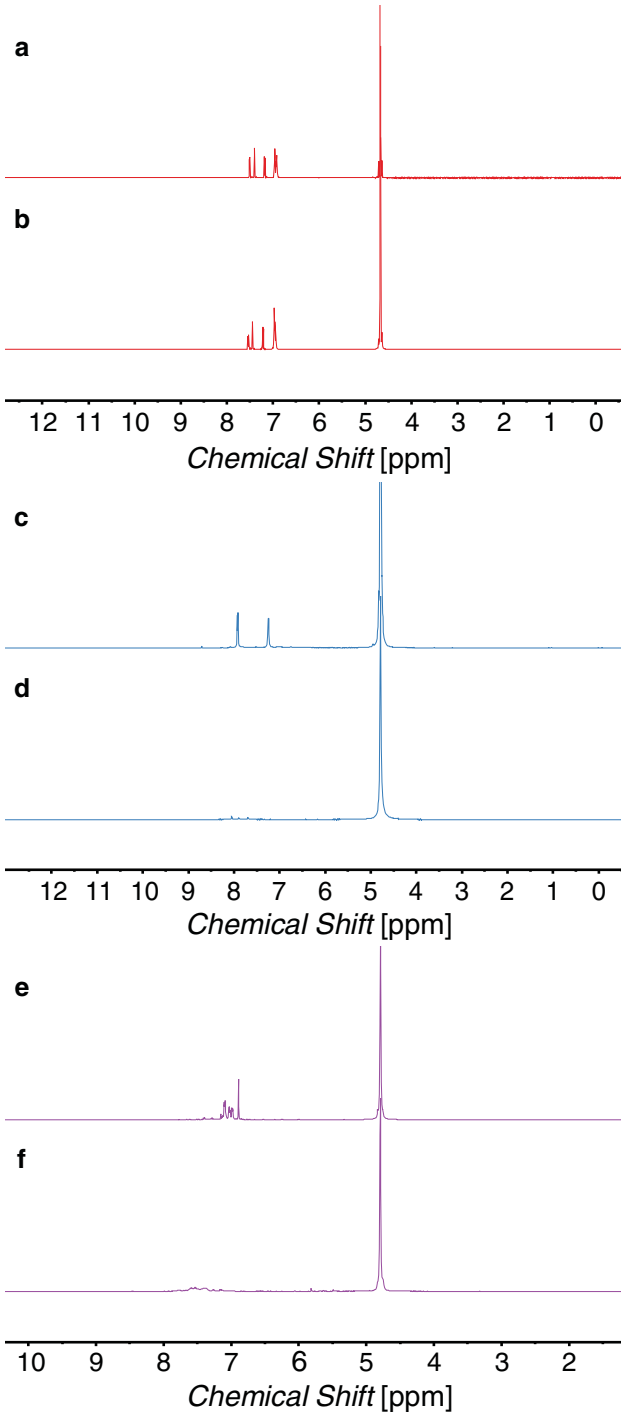

Figure 3. a) Proton NMR of AQS without bromine and b) after adding bromine and allowing the sample to sit for 24 h . No change was observed. Proton NMR of DHAQDS c) before and d) after addition of bromine. Proton NMR of ARS e) before and f) after addition of bromine. The disappearance of the aromatic proton peaks in the 7.0–8.0 ppm range indicates the consumption of DHAQDS and ARS. The peak at 4.8 ppm is from the solvent.

50 mA cm^{-2} accesses more than 75% of the theoretical capacity of the AQDS and AQS solutions, with high current efficiency (>99%) and negligible capacity fade for the AQDS cell. Although the AQS cell appears to lose capacity during the experiment,

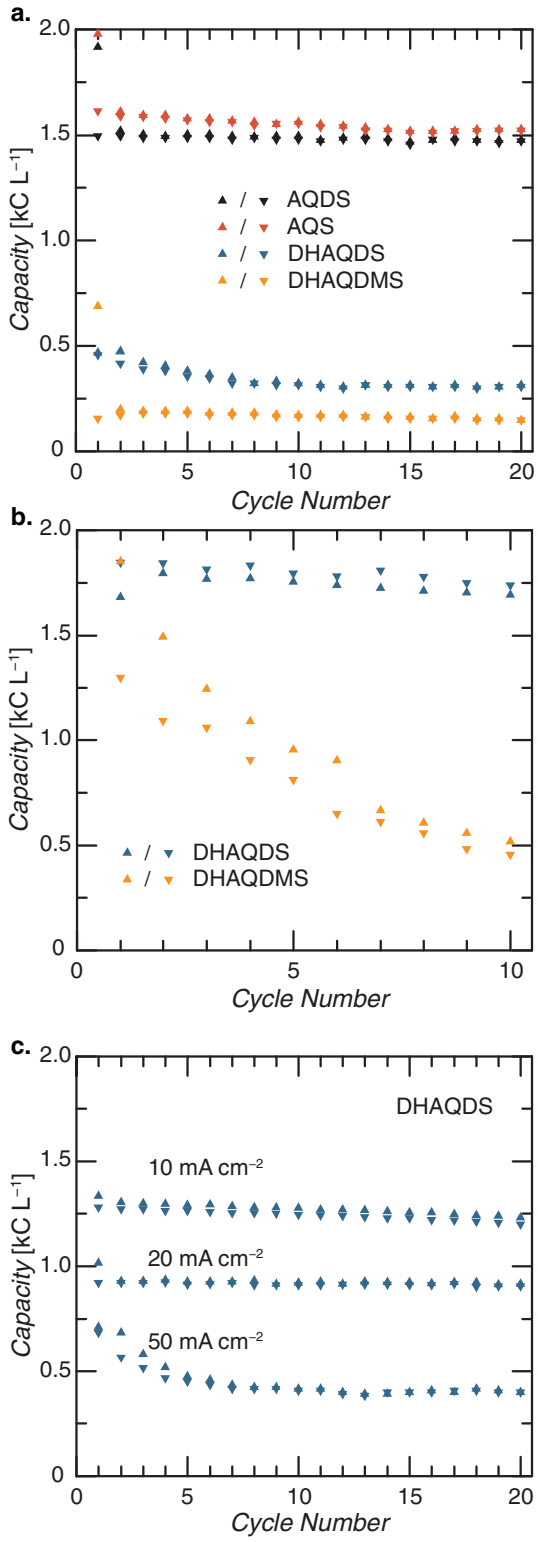

Figure 4. a) Cycling capacity of each quinone test solution during constant-current cycling at 50 mA cm^{-2}. b) Cycling capacity of the DHAQDS and DHAQDMS solutions during constant-voltage cycling. c) Cycling capacity of the DHAQDS solution at different rates, demonstrating the dependence of accessible capacity on cycling rate. Upward-pointing triangles represent charge capacity and downward-pointing triangles represent discharge capacity.

constant voltage holds before and after the constant-current cycling experiment show identical discharge capacities, indicating no loss of redox-active species (Figure S3, Supporting Information). DHAQDS and DHAQDMS solutions, on the other hand, fail to attain charge/discharge capacities close to the theoretical value for 20 mL of a 0.01 M solution (≈2 kC L^{-1}) at this cycling rate. Constant-voltage cycling between voltage limits of +0.4 and −0.2 V (Figure 4b) shows that the majority of the capacity of the DHAQDS solution is accessible given enough time, or a slow enough rate. Differences in the charging and discharging rates during these constant-voltage cycles indicate that the oxidation of reduced DHAQDS (the discharge reaction) is sluggish, which limits the rate at which the DHAQDS solution can be cycled at constant current. The discharge capacity measured this way is often slightly larger than the charge capacity; this is likely due to the gradual crossover of reduced and oxidized AQDS from the posolyte increasing the capacity of the DHAQDS solution over time. Additionally, slowing the rate of constant-current cycling (Figure 4c) accesses more of the capacity of the DHAQDS solution. Therefore, we conclude that DHAQDS can be reduced and re-oxidized but, even at high concentration may require higher surface area electrodes, or a catalyst, to enable high-current-density operation.

DHAQDMS, in contrast, shows rapid capacity fade in the constant voltage cycling. We hypothesize that the reduced form of DHAQDMS undergoes a decomposition reaction slower than the time scale of the cyclic voltammogram in Figure 1a, but faster than the cycles in Figure 4. Thus, under the conditions reported herein, DHAQDMS does not appear to be electrochemically cyclable.

5. AQS-Bromide Flow Cell

Flow batteries using an AQS negolyte gain about 80 mV in open circuit potential over AQDS-based flow batteries with the same posolyte, without sacrificing aqueous solubility—both molecules are soluble to at least 1 M in their acid forms. An increase in OCV can allow for higher power density or offset additional voltage losses caused by switching molecules. Voltage losses are generally associated with sluggish electrochemical kinetics, Ohmic resistance effects, or slow mass transport, and each of these losses uniquely affects the cell's polarization curve.[18] To investigate these voltage losses, we obtained polarization curves (Figure 5) from AQDS and AQS flow cells with identical quinone concentrations (1 M), negolyte proton concentrations (3 M), posolytes (3 M HBr, 0.5 M Br_2), and cell hardware (see the Experimental Section). Kinetic losses would manifest themselves as changes of slope of the polarization curve near zero current density. Neither the AQS nor the AQDS cell shows signs of kinetic losses, due to the rapid redox kinetics of the quinones[6,7] and the bromine/hydrobromic acid couple.[1] Mass transport losses, in the traditional sense of a limiting current density causing a precipitous drop in cell voltage, are not observed, possibly due to the use of an interdigitated flow field with high flow rates in each cell. Under these experimental conditions, the electrolyte flowed at ≈20 times stoichiometric flow. Therefore, it is unsurprising that limiting currents are not apparent in the polarization

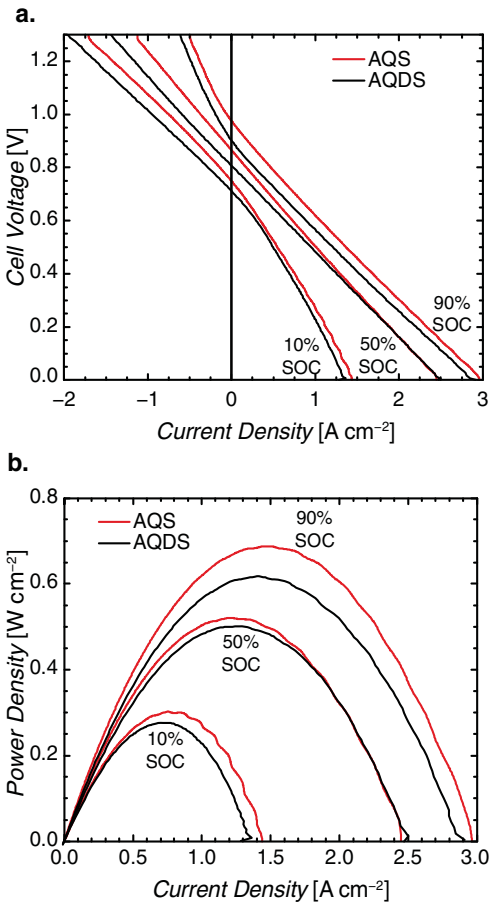

Figure 5. a) Polarization curves and b) galvanic power density for AQS-bromide and AQDS-bromide cells with identical quinone concentrations, negolyte proton concentrations, posolytes, and cell hardware. The AQS cell exhibits higher open circuit voltage and power density. Both cells have nearly linear polarization curves, indicating predominantly resistive losses during operation.

curves. At extreme states of charge (10% and 90%), the polarization curves deflect from linearity in both cells at relatively low current. Such an effect could be explained by a shift in the physical location of the electrochemical reaction away from the membrane due to local depletion of reactants. If the reaction zone shifts, the distribution of electronic and ionic current within the porous electrode will shift, possibly resulting in greater overpotentials from ionic current conduction in the electrolyte. The nearly linear polarization curves at 50% state of charge (**Figure 5**a) indicate that resistive losses dominate the behavior of both cells. As can be seen by the slopes of the polarization curves, the resistance of the AQS cell at intermediate and high state of charge was slightly higher than that of the AQDS cell: evaluated by fitting a line over the entire measured current range at 50% state of charge, these polarization resistances were 357 mΩ cm^2 for the AQS cell and 331 mΩ cm^2 for the AQDS cell. The origin of this resistance difference is not clear. Electrolyte conductivity measurements (see the Supporting Information) show that the AQS electrolyte is slightly more conductive than the AQDS electrolyte: 0.56 S cm^{-1} for AQS versus 0.51 S cm^{-1} for AQDS. Therefore, another effect must be contributing to the increase in cell resistance, such as an increase in the membrane resistance caused by slightly different electrolyte environments in each cell (see the Experimental Section). The slight increase in cell resistance for AQS contributes an additional 26 mV of loss for each A cm^{-2} increase in current density. This loss, however, is offset by an average 80 mV increase in open circuit potential for the AQS cell over that of the AQDS cell, meaning that AQS cells still exhibit higher voltage than AQDS cells. The increased open circuit potential results in a peak galvanic power density for the AQS cell of 0.7 W cm^{-2} at 90% state of charge (Figure 5b), which is the highest reported to date for a quinone-based flow cell at room temperature.

5.1. Cycling of AQS-Bromide Flow Battery

An AQS-bromide flow battery was cycled at constant current at 0.25 A cm^{-2}. Additional sulfuric acid was used in the posolyte (3 M HBr, 0.5 M Br_2, 0.5 M H_2SO_4), in comparison to the AQS cell described previously, in order to reduce water crossover arising from osmotic imbalance during cycling. The average current efficiency over these 15 cycles was 96.5% and the average energy efficiency 73.5% (**Figure 6**). This energy efficiency is an improvement over AQDS cells, which have reported energy efficiency of 62% at the same current density at room temperature with a nearly identical posolyte (3.5 M HBr, 0.5 M Br_2).[11] The loss of current efficiency in hydrogen-bromine[19] and quinone-bromine[11] cells has been attributed quantitatively to bromine crossover through the Nafion membrane. Although the efficiencies are promising, the cell's capacity fade is currently too great for practical usage, at ≈1% capacity loss per cycle. This capacity fade is on par with other proof-of-concept organic RFBs, including AQS-tiron[7] and 4-hydroxy-2,2,6,6-tetramethylpiperidin-1-oxyl (4-HO-TEMPO)-methyl viologen[20] but, prior to practical implementation, more needs to be done to identify the origin of this capacity fade and minimize it.[21]

6. Conclusion

The chemical tunability of quinones provides a unique tool for designing flow battery electrolytes for cost-effective grid-scale storage. Many anthraquinone derivatives are potential negolyte materials, but only a subset of those can be used in bromine-based batteries.

Though DHAQDS has a desirably low reduction potential, its irreversible reaction with bromine precludes its use in a bromine-containing RFB. Nevertheless, the dilute concentration cycling experiments against AQDS show promise for DHAQDS in an RFB utilizing a bromine-free posolyte. The relatively sluggish oxidation kinetics of its reduced form will have to be addressed for operation at high current density.

Conversely, DHAQDMS has the lowest reduction potential of all the molecules we evaluated, as well as apparent stability against bromine substitution; however, reversible reduction of the molecule does not occur under the acidic conditions commonly encountered in a bromine-based flow battery.

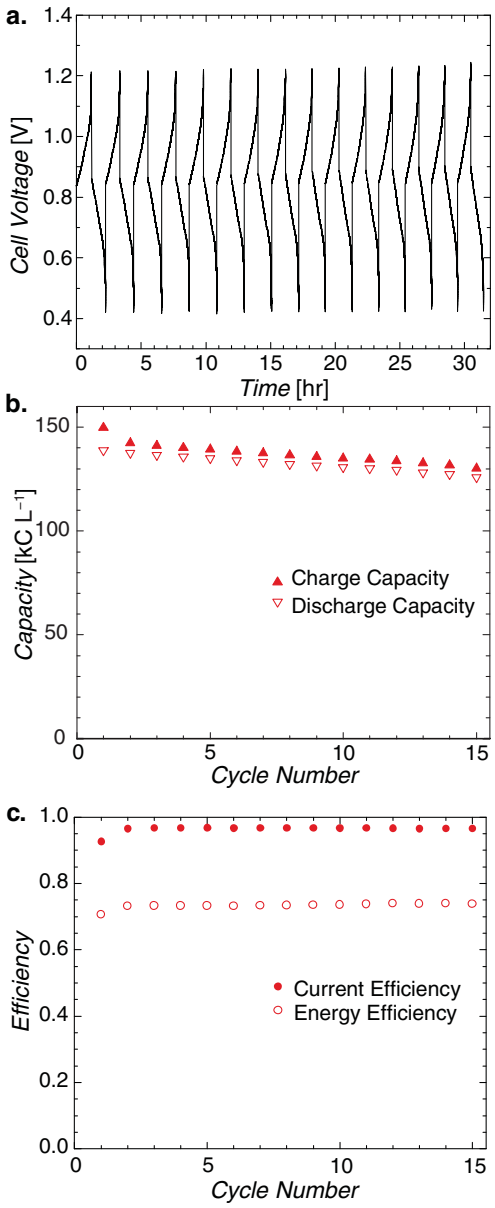

Figure 6. a) Voltage versus time, b) charge/discharge capacities, and c) current and energy efficiencies for constant current cycling of an AQS-bromide flow battery at 0.25 A cm^{-2}.

AQS is stable in bromine and can be cycled in a quinone-bromide flow battery. The AQS-bromide RFB exhibits a higher OCV than a comparable battery utilizing AQDS, while maintaining rapid redox kinetics. Thus, despite slightly higher cell resistance, AQS-bromide cells show an increased peak galvanic power density over AQDS cells. These modest performance advantages make AQS a serious candidate for further development of quinone-bromide RFBs. Presumably, the removal of a sulfonate group from AQDS to AQS should lower the aqueous solubility of the molecule. Nevertheless, we have placed a lower bound of 1 M on the solubility of protonated AQS, equivalent to 2 M electrons and comparable to vanadium flow batteries, which operate in the 2–3 M range.

Table 2. Comparison of anthraquinone derivatives as negolyte candidates.

Molecule	Standard reduction potential [V vs SHE]	Stability against bromination	Stability upon reduction
AQDS	0.210	Good	Good
AQS	0.187	Good	Good
DHAQDS	0.120	Poor	Good
ARS	0.082[a)]	Poor	Good[a)]
DHAQDMS	0.020	Apparently stable	Poor

[a)]Obtained from ref. [17].

Long-term stability, if different between the two molecules, may ultimately be the decisive factor. These results are summarized in **Table 2**.

7. Experimental Section

Electrolyte Preparation: AQS electrolyte solution was prepared by passing anthraquinone-2-sulfonic acid sodium salt (97% dry wt, Alfa Aesar) through an ion exchange column (see the Supporting Information) to yield the protonated form. DHAQDS and DHAQDMS[22] were synthesized as described in the Supporting Information. Negolyte solutions of 1 M concentration were prepared for each quinone. Sulfuric acid (95%–98%, Sigma Aldrich) was added in enough quantity to give the desired final concentration of sulfuric acid in the negolyte: 2 M for AQS, 1 M for AQDS, DHAQDS, or DHAQDMS, resulting in 3 M protons in all cases. Bromine (98%, Alfa Aesar) and hydrobromic acid (48%, Alfa Aesar) were used as received and diluted with deionized water (18.2 MΩ, Millipore) to produce a posolyte solution of 3 M hydrobromic acid, 0.5 M bromine.

Computational Methods: Density functional theory was used to assess the susceptibility of quinones to irreversible electrophilic aromatic addition by bromine. Global reaction energies (ΔE_R) and intermediate formation energies (ΔE_{int}) were calculated as the difference in energy between reactants and products (at 0 K) for the final bromination product and the high-energy addition intermediate, respectively. Each C—H position of both the reduced and oxidized quinones was considered as a potential reaction site. Initial geometry guesses were generated automatically using a random distance-matrix approach at the MMF94 level of theory[23] and were subsequently refined at the PBE/6-31G* and B3LYP/6-31G* levels of theory using Terachem.[24] To correct systematic errors in our approach, to account for the unknown molecular nature of the brominating reactant, and for easier comparison, all values are reported as difference values with AQDS as a reference.[24]

Bromine Reactivity Test: A dry 50 mg sample of each species was dissolved in 0.8 mL of deuterated water, and ^{1}H NMR spectra were taken (see the Supporting Information). Each sample was exposed to bromine by dropping 0.1 mL bromine into the sample and letting it stand for 24 h. NMR spectra were again recorded.

Electrochemical Experiments: All electrochemical experiments were performed on a Gamry Reference 3000 potentiostat. A Gamry Reference 30 K booster was included for all flow cell tests. Nafion 212 membranes were cut to 9 cm^2 and soaked in deionized water at room temperature for at least 24 h before use in a cell. Sigracet 10-AA electrodes (SGL Group) were cut to 5 cm^2 and baked in air for 24 h at 400 °C before use in a cell.

Cyclic voltammetry experiments were performed with 1×10^{-3} M quinone solutions with 1 M sulfuric acid supporting electrolyte. The

working electrode was a glassy carbon disk (BASi), 3 mm diameter, polished with 50 nm alumina slurry (Electron Microscopy Sciences) for ≈30 s. A silver/silver chloride reference electrode (BASi, +0.210 V vs SHE, 3 M NaCl filling solution) and a platinum coil counter electrode were also used. The potential of the working electrode began at open circuit and was swept negative, then positive, at 25 mV s^{-1}.

Flow Cell Experiments: The flow cell consisted of a 9 cm^2 sheet of Nafion 212 membrane, sandwiched between three sheets of Sigracet 10 AA electrodes (uncompressed thickness 400 µm) on each side. A Teflon gasket (0.002 in. thickness) surrounded the Nafion membrane, while Teflon gaskets of 0.032 in. thickness surrounded the electrodes. Pyro-sealed graphite flow plates (Fuel Cell Technologies) with interdigitated flow channels were used to disperse fluid into the porous electrodes. Six 3/8 in. 24 bolts torqued to 90 in. lbs held the cell together. Polytetrafluoroethylene (PTFE) reservoirs (Savillex) housed the electrolytes, which were circulated through perfluoroalkoxy alkane (PFA) tubing (McMaster-Carr) to the cell by Cole-Parmer PTFE diaphragm pumps at a 100 mL min^{-1} flow rate (50 RPM). All cells used 35 mL of the quinone electrolyte and 42 mL of the bromine electrolyte.

The diaphragm pumps result in pulsing flow, which complicates the recording of polarization curves. A voltage sweep began at the cell's open circuit potential, swept positive to 1.3 V, negative to 0 V, and back to open circuit, at a rate of 100 mV s^{-1}. The measured current response oscillated due to the pulsed flow, so a moving average filter of width equivalent to the pulse period (1.2 s) was applied to the data. After filtering the data, the polarization curves often showed a hysteresis: the forward and backward traces differed by about 20 mV. This difference is likely due to changing the state of charge of the cell, as the amount of charge passed is about 5% of the total cell capacity. Therefore, the authors report the average of the forward and backward voltage sweeps.

Quinone-AQDS Flow Cell Cycling: The flow cell was constructed as described above. A 1 M AQDS, 1 M sulfuric acid solution (30 mL) was electrochemically reduced in the cell, using a posolyte consisting of 1 M tiron and 1 M sulfuric acid (1,2-hydroquinone-3,5-disulfonic acid, Alfa Aesar). The cell was charged at 0.9 V until 3000 Coulombs of charge passed, which is enough to reduce 52% of the AQDS.

Four separate testing electrolytes were prepared, one for each of the four quinones (AQDS, AQS, DHAQDS, and DHAQDMS). These testing electrolytes contained 0.01 M quinone and 3 M sulfuric acid. The tiron electrolyte was drained from the cell and replaced with 20 mL of each of the four electrolytes in succession. Prior to each test, the testing electrolytes were degassed with argon. During each test, the testing electrolyte was kept under positive pressure of argon gas. Before cycling, constant voltage holds of ±0.3 V (+0.4 V/−0.2 V for DHAQDS and DHAQDMS) for 600 s were used to charge and discharge the cell to ensure the cell could achieve its predicted charge/discharge capacity. Each testing electrolyte was cycled against the 1 M AQDS electrolyte at 50 mA cm^{-2} constant current for 20 cycles with voltage cutoffs of ±0.3 V (+0.4 V/−0.2 V for DHAQDS and DHAQDMS). The high-concentration, high-volume AQDS posolyte ensures the testing electrolyte is capacity limiting. Therefore, the authors report charge and discharge capacities normalized by the testing electrolyte volume.

Constant voltage cycling of DHAQDS and DHAQDMS electrolytes was performed by alternating voltage holds of +0.4 V for 600 s and −0.3 V for 2400 s. The reported capacity is the integration of the current over the duration of the experiment.

AQS-Bromide Flow Cell Cycling: The flow cell was constructed as described above. The negolyte (35 mL) consisted of 1 M AQS, ion exchanged as described above, and 2 M H_2SO_4. The posolyte (42 mL) consisted of 3 M HBr, 0.5 M Br_2, and 0.5 M H_2SO_4. The additional sulfuric acid slows water crossover from posolyte to negolyte during cycling by correcting for osmotic imbalances. The additional posolyte ensures the negolyte is capacity limiting. Therefore, the authors report charge and discharge capacities normalized by the negolyte volume.

The cell was cycled at 0.25 A cm^{-2} constant current, beginning with a charge. A charging cutoff of 1.3 V and a discharging cutoff of 0.3 V were used to prevent side reactions. When the cell reached these cutoff voltages during the corresponding charging or discharging step, the current was reversed, beginning the subsequent discharging or charging step.

Supporting Information

Supporting Information is available from the Wiley Online Library or from the author.

Acknowledgements

This work was partially funded through the US Department of Energy ARPA-E Award DE-AR0000348 and partially funded through the Harvard John A. Paulson School of Engineering and Applied Sciences. This work was also supported by funding from the Massachusetts Clean Energy Technology Center. R.G.B. acknowledges the use of the Harvard FAS Odyssey Cluster and support from FAS Research Computing. The authors thank Kaixiang Lin, Eugene Beh, Marc-Antoni Goulet, Sergio Granados-Focil, Lauren Hartle, Louise Eisenach, and Andrew Wong for helpful discussions on chemical synthesis and experimental electrochemical techniques. The authors also thank Eugene Beh for assistance in proofreading the manuscript. The authors thank Süleyman Er and Changwon Suh for theoretical discussions. Rachel Burton assisted in synthesis procedures.

Received: July 8, 2016
Revised: October 17, 2016
Published online:

[1] A. Z. Weber, M. M. Mench, J. P. Meyers, P. N. Ross, J. T. Gostick, Q. Liu, *J. Appl. Electrochem.* **2011**, *41*, 1137.
[2] B. R. Chalamala, T. Soundappan, G. R. Fisher, M. R. Anstey, V. V. Viswanathan, M. L. Perry, *Proc. IEEE* **2014**, *102*, 1.
[3] M. Skyllas-Kazacos, G. Kazacos, G. Poon, H. Verseema, *Int. J. Energy Res.* **2010**, *34*, 182.
[4] G. Kear, A. A. Shah, F. C. Walsh, *Int. J. Energy Res.* **2012**, *36*, 1105.
[5] a) B. Huskinson, S. Nawar, M. R. Gerhardt, M. J. Aziz, *ECS Trans.* **2013**, *53*, 101; b) K. Lin, Q. Chen, M. R. Gerhardt, L. Tong, S. B. Kim, L. Eisenach, A. W. Valle, D. Hardee, R. G. Gordon, M. J. Aziz, M. P. Marshak, *Science* **2015**, *349*, 1529; c) B. Yang, L. Hoober-Burkhardt, S. Krishnamoorthy, A. Murali, G. K. S. Prakash, S. R. Narayanan, *J. Electrochem. Soc.* **2016**, *163*, A1442.
[6] B. Huskinson, M. P. Marshak, C. Suh, S. Er, M. R. Gerhardt, C. J. Galvin, X. Chen, A. Aspuru-Guzik, R. G. Gordon, M. J. Aziz, *Nature* **2014**, *505*, 195.
[7] B. Yang, L. Hoober-Burkhardt, F. Wang, G. K. Surya Prakash, S. R. Narayanan, *J. Electrochem. Soc.* **2014**, *161*, A1371.
[8] S. Er, C. Suh, M. P. Marshak, A. Aspuru-Guzik, *Chem. Sci.* **2015**, *6*, 885.
[9] Q. Chen, M. R. Gerhardt, L. Hartle, M. J. Aziz, *J. Electrochem. Soc.* **2015**, *163*, A5010.
[10] M. L. Perry, R. M. Darling, R. Zaffou, *ECS Trans.* **2013**, *53*, 7.
[11] Q. Chen, L. Eisenach, M. J. Aziz, *J. Electrochem. Soc.* **2015**, *163*, A5057.
[12] B. Huskinson, M. P. Marshak, M. R. Gerhardt, M. J. Aziz, *ECS Trans.* **2014**, *61*, 27.
[13] S. Bailey, I. Ritchie, *Electrochim. Acta* **1985**, *30*, 3.
[14] M. C. Tucker, K. T. Cho, A. Z. Weber, G. Lin, T. Van Nguyen, *J. Appl. Electrochem.* **2014**, *45*, 11.

[15] G. S. Hammond, *J. Am. Chem. Soc.* **1955**, *77*, 334.
[16] J. Criquet, E. M. Rodriguez, S. Allard, S. Wellauer, E. Salhi, C. A. Joll, U. von Gunten, *Water Res.* **2015**, *85*, 476.
[17] S. Zhang, X. Li, D. Chu, *Electrochim. Acta* **2016**, *190*, 737.
[18] D. Aaron, Z. Tang, A. B. Papandrew, T. a. Zawodzinski, *J. Appl. Electrochem.* **2011**, *41*, 1175.
[19] K. T. Cho, M. C. Tucker, M. Ding, P. Ridgway, V. S. Battaglia, V. Srinivasan, A. Z. Weber, *ChemPlusChem* **2015**, *80*, 402.
[20] T. Liu, X. Wei, Z. Nie, V. Sprenkle, W. Wang, *Adv. Energy Mater.* **2016**, *6*, 1501449.
[21] T. B. Schon, B. T. McAllister, P. F. Li, D. S. Seferos, *Chem. Soc. Rev.* **2016**, *45*, 6345.
[22] R. J. Ardecky, D. Dominguez, M. P. Cava, *J. Org. Chem.* **1982**, *47*, 409.
[23] J. P. Ebejer, G. M. Morris, C. M. Deane, *J. Chem. Inf. Model.* **2012**, *52*, 1146.
[24] I. S. Ufimtsev, T. J. Martinez, *J. Chem. Theory Comput.* **2009**, *5*, 2619.

Supporting Information

Anthraquinone Derivatives in Aqueous Flow Batteries

Michael R. Gerhardt, Liuchuan Tong, Rafael Gómez-Bombarelli, Qing Chen, Michael P. Marshak, Cooper J. Galvin, Alán Aspuru-Guzik, Roy G. Gordon, and Michael J. Aziz *

1. Supplemental Methods

1.1 Ion exchange

A glass ion exchange column was filled with Amberlyst® 15(H) ion exchange resin (Alfa Aesar). A 1 M hydrochloric acid solution was prepared concentrated stock (37%, Sigma Aldrich) diluted with deionized water (18.2 MΩ, Millipore). This hydrochloric acid solution was used to activate the column prior to passing an anthraquinone solution through the column. After passing through the column, the ion-exchanged anthraquinone solution was evaporated to dryness on a hot plate at approximately 100 °C and redissolved in deionized water. Solution was passed successively through medium and fine porosity glass frit filters to remove insoluble material.

1.2 Synthesis of 1,8-dihydroxyanthraquinone-2,7-disulfonic acid

Fuming sulfuric acid (68 ml, 20 % SO_3 content, Alfa Aesar) was added to 1,8-dihydroxyanthraquinone (40 g, 165.3 mmol, TCI) in an oven-dried round-bottom flask, and the flask was covered with a watch glass. The mixture was heated to 180 °C overnight while stirring. After cooling to room temperature, the reaction mixture was poured into cold water (200 ml) and NaCl brine (100 mL) was added. A brown precipitate formed, which was filtered, washed with brine (3 x 100 mL) and rapidly washed with cold water (50 mL). The resulting precipitate was vacuum dried without further purification to provide 70 g (95%

yield) of 1,8-dihydroxyanthraquinone-2,7-disulfonate disodium salt. The protonated form was obtained by the ion exchange procedure defined above.

1.3 Synthesis of 1,4-dihydroxyanthraquinone-2,3-dimethylsulfonic acid: Sodium sulfite (2.96g, 23.5 mmol) and potassium iodide (195 mg, 1.17 mmol) were added to a solution of 1,4-dihydroxy-2,3-bis(bromomethyl)anthraquinone (5 g,11.74 mmol, prepared according to Ref. [22]) in water/acetonitrile (100 mL, 5:1 v/v). The mixture was refluxed under nitrogen atmosphere for 18 hours, and cooled to room temperature. The mixture was then passed through an ion exchange column filled with Amberlyst® 15(H) ion exchange resin (Alfa Aesar) activated with 1 M hydrochloric acid. The resulting solution was concentrated by vacuum drying to produce 3.3 g (66% yield) of 1,4-dihydroxy-anthraquinone-2,3-dimethylsulfonic acid. [22] HRMS (ESI) *m/z*: calcd for $C_{16}H_{11}O_{10}S_2$, $[M - H]^-$, 426.9799; found, 426.9803.

1.4 Proton nuclear magnetic resonance

^{1}H NMR spectra were recorded using Varian INOVA 500 (500 MHz) NMR spectrometers at 23 °C. Proton chemical shifts are expressed in parts per million (ppm, δ scale) and are referenced to residual ^{1}H in the NMR solvent ($CDCl_3$, δ 7.26 ppm; $(CD_3)_2SO$, 2.50 ppm).

1.5 Electrolyte conductivity measurements

Electrolyte conductivity measurements were performed using a custom-built conductivity cell comprising a length of ¼ inch wide PFA tubing, approximately 8.5 cm long with a 1/8 inch inner diameter, two T-shaped PVDF push-to-connect fittings, and two ¼ inch diameter niobium rods for electrodes. Galvanostatic electrochemical impedance spectroscopy (EIS) was performed using a Gamry Reference 3000 potentiostat, sweeping from 1 MHz to 100 Hz with 0.01 A rms applied AC current. The conductivity cell was calibrated with 1 M and 0.1 M potassium chloride solutions and found to have an L/A constant of 109 ± 1 cm^{-1}.[25] Impedances with a phase value between 2 and −2 degrees were averaged to calculate the

solution resistance. Dividing the cell L/A constant by the resistance gives the electrolyte conductivity. Nyquist plots are shown in **Figure S1**.

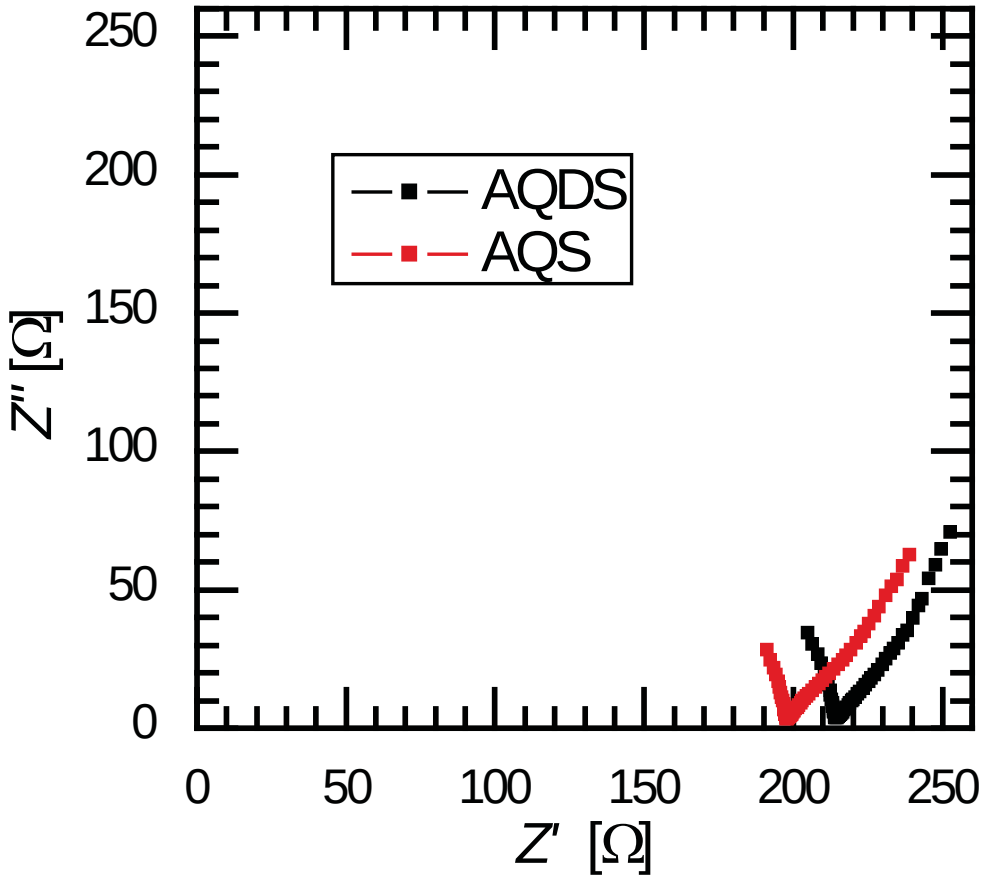

Figure S1. Nyquist plots for AQDS and AQS electrolytes (1 M quinone, 3 M total proton content, additional protons provided by sulfuric acid). Electrolyte conductivities were 0.51 S cm^{-1} for AQDS and 0.55 S cm^{-1} for AQS.

2. Quinone stability to electrochemical cycling – voltage profiles

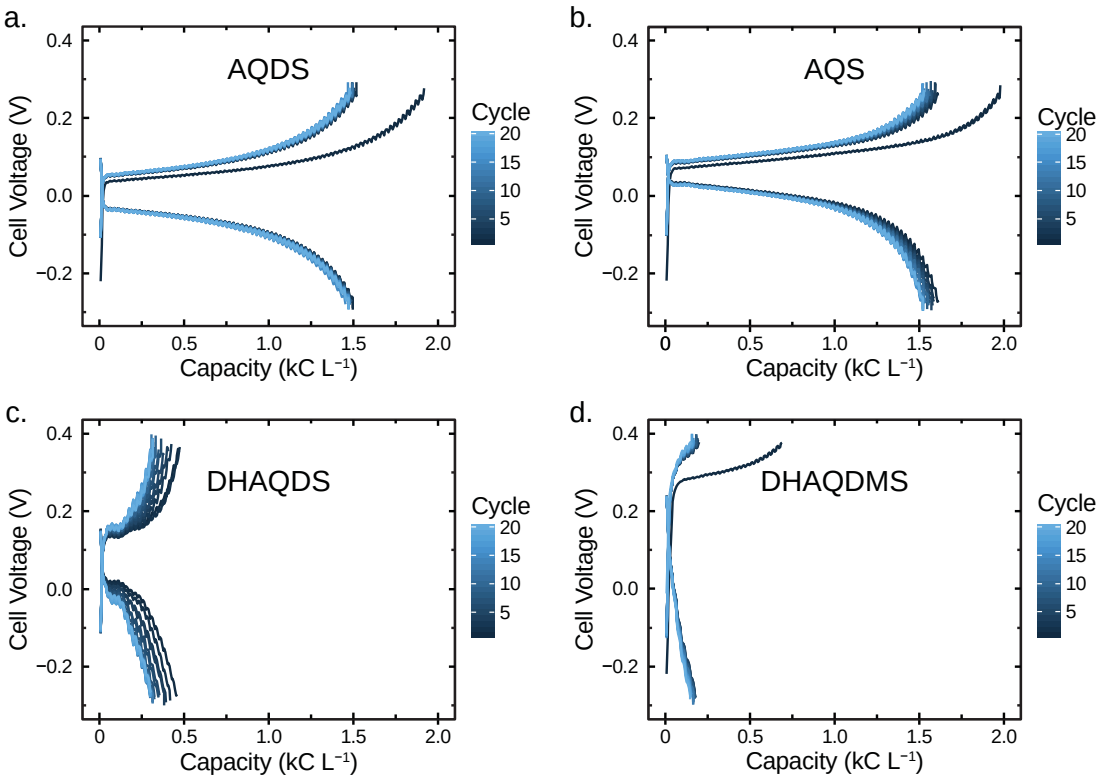

Figure S2. Voltage profiles for constant-current cycling experiments of each of the four molecules studied against an AQDS-H_2AQDS electrolyte. All cycling was performed at 50 mA cm^{-2}. The voltage oscillations in the figures are a result of pulsating flow from the diaphragm pumps used to circulate the electrolyte. These oscillations are enhanced due to the low concentration (0.01 M) of quinone, resulting in test cells which are extremely sensitive to mass transport conditions. The drop in capacity from cycle 1 to 2 in the AQDS and AQS cells can be explained by an inability to fully discharge the cell after the first full charge, due to these mass transport limitations. Constant voltage holds (figure S3) demonstrate little to no capacity fade after these 20 cycles.

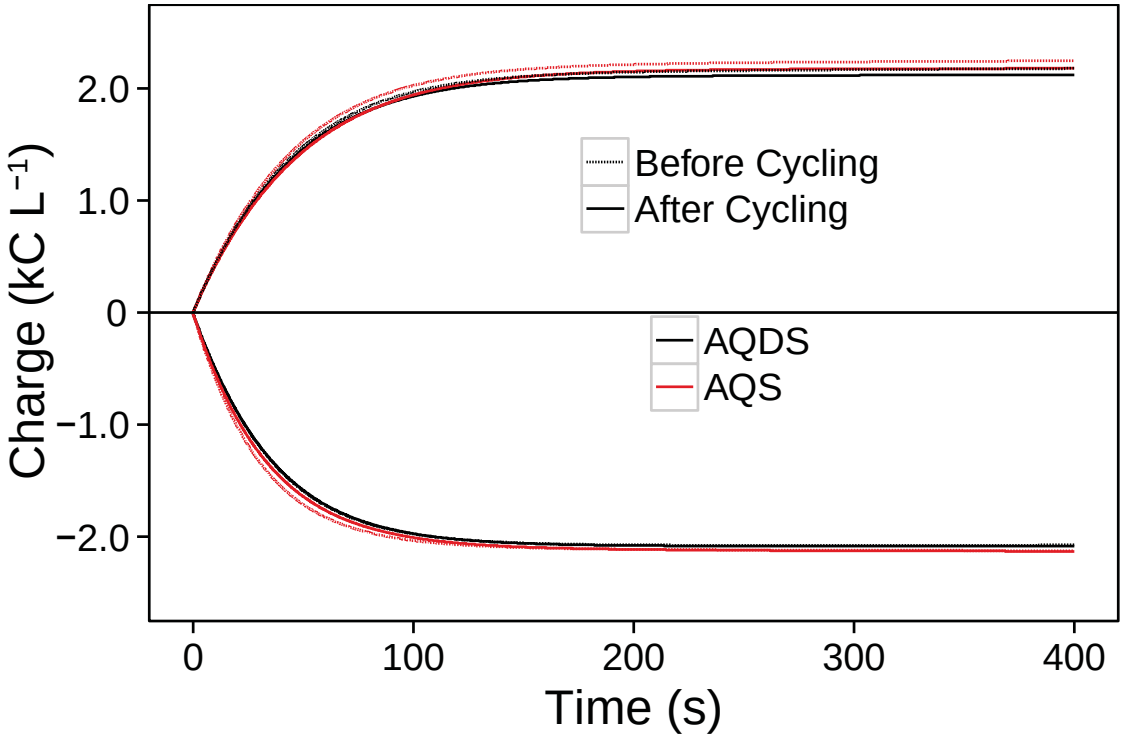

Figure S3. Constant voltage charging/discharging of AQDS and AQS low-concentration electrolytes immediately prior to or following the constant-current cycling shown in figures 4a and S2. The cell was charged at 0.3 V and discharged at −0.3 V. These results demonstrate little to no capacity fade in either cell, provided enough time is given for the cell to charge and discharge.